RSC Advances

PAPER

Cite this: *RSC Adv.*, 2019, **9**, 13054

A facile method for fabricating a three-dimensional aligned fibrous scaffold for vascular application†

Feng Lin Ng,[ab] Yee Oon Ong,[a] Hui Zhi Chen,[a] Le Quan Ngoc Tran,[b] Ye Cao,[a] Bee Yen Tay[b] and Lay Poh Tan*[a]

Received 25th January 2019
Accepted 5th April 2019

DOI: 10.1039/c9ra00661c

rsc.li/rsc-advances

Vascular graft replacement remains the optimal treatment option for many vascular diseases despite advances in endovascular surgery. In this study, we proposed the use of surface topographical cues to align and maintain the phenotype of vascular smooth muscle cells (vSMCs) which were reported as one of the vital limitations for successful graft replacement. An auxiliary electrospinning setup has been developed to collect circumferentially aligned fibres on a 3D tubular format; this micro-architecture was found to be similar to the tunica media layer of blood vessels. The presence of aligned fibres served as a signaling modality to induce cell alignment and the maintenance of the contractile phenotype. vSMCs cultured on the 3D aligned fibrous substrate were found to exhibit better cell proliferation ability and enhanced cell-shape directionality. The functional expression of the two representative intracellular contractile proteins (*i.e.* α-SMA and MHC) was found to exhibit definitive markers that are orderly organized as microfilament bundles. Collectively, the result suggests a possibility of adapting the 3D aligned tubular scaffold to enhance and regulate cell function along with the additional tunability of scaffold diameter and thicknesses for tailoring to the needs of individual patients or future *ex vivo* studies.

Introduction

Vascular tissue engineering is an essential research arena considering that cardiovascular disease is one of the world leading causes of death, with more than 30% of deaths worldwide attributed to it.[1] Although blood vessel transplantation such as Dacron® and expanded polytetrafluoroethylene is widely used for vascular treatment, it is often limited to large vessels (*e.g.* > 6 mm in diameter).[2] In addition, many synthetic vascular transplants present several limitations such as aneurysms, thrombosis and graft failure.[3] This leaves autografts as the current gold standard for the repair of blood vessels, especially small caliber arteries with diameter <6 mm.[4,5] However, autografts have other limitations such as donor site morbidity, inherent size mismatch, and potential vascular pathologies[6,7] resulting in an increasing need for this area of research.

Recent studies suggested that many vascular pathologies are attributed to the excessive proliferative nature of smooth muscle cells (SMCs).[8,9] Smooth muscle cells when loses its contractile protein and quiescence state will undergo increased proliferation, migration and produce excessive extracellular matrix (ECM) proteins and pro-inflammatory cytokines and growth factors which eventually lead to deadly vascular diseases.[8,10] Several research group have made attempts to modulate the phenotype of vascular smooth muscle cells through approaches such as micro-patterning,[9,11,12] electrospinning,[13–15] coating of heparin[8,16] or having endothelial cells (ECs) on the inner side of scaffold.[10,16,17] While micro-patterning creates a defined cellular monolayer of cells, it rapidly loses its regularity when translated into multiple layers.[12,18] This 2D nature of micro-patterned cellular sheets presents a major limitation for tissue engineering, where the assembly of thick multi-component cell construct is desired. On the other hand, coating of heparin[19,20] was reported to aid in the reduction of thrombosis, however it loses its effect rapidly to plasma. Differing reports were also made on the role of endothelial cells on modulating SMC behavior.[8,21,22] It was found that neither the simple presence nor absence of endothelial cells will promote the quiescence state of SMC. It is the appropriate environment that must be provided to ECs and SMCs to achieve control of SMC phenotype thereby increased graft patency.[8,21]

To date, a number of studies have successfully demonstrated the development of vascular graft either through electrospinning,[13,14,23] braiding,[4] melt spinning[24] or a combination of fabrication technique to mimic the various layer of vascular graft.[4,15,25,26] While these approaches demonstrated the maintenance of smooth muscle cells[13] or endothelial cells[22,27] along with improved graft patency in *in vivo* models; these scaffolds presented were mainly for larger caliber,[15,25] with limited thickness and porosity,[4,14] and the absence of fibres aligned

[a]*School of Materials Science & Engineering, Nanyang Technological University, N4. 1-01-07, 50 Nanyang Avenue, Singapore 639798, Singapore. E-mail: lptan@ntu.edu.sg*
[b]*Singapore Institute of Manufacturing Technology, 73 Nanyang Drive, Singapore 637662, Singapore*

† Electronic supplementary information (ESI) available. See DOI: 10.1039/c9ra00661c

circumferentially along the tubular scaffold. Knowing that the tunica media layer is the muscular middle layer of arteries comprising mainly of smooth muscle cells aligned circumferentially along blood vessel, we hypothesized that a substrate with three-dimensional nature and fibres aligned along the circumference of the tubular scaffold is highly relevant. Considering the requirement of fiber alignment on smooth muscle cell function along with sufficient substrate thickness for tissue remodeling, an innovative setup is needed to address the current limitation.

It has been widely reported that topographical cues *e.g.*, alignment of fibers can direct cell orientation, proliferation and differentiation.[18,28] In this context, we adopted the use of electrospinning to modulate the behavior of SMCs by inducing the orientation and phenotype that mimic the tunica media architecture. Electrospinning has been considered as the favorable method for producing nanofibrous structure since the fibres produced closely mimics the ECM architecture.[29–31] However, the conventional electrospinning setup is limited to 2D nature, with fibers collected often in a random and dense state.[29] Thus, an auxiliary setup for electrospinning has been designed in this study for the collection of 3D aligned nanofibers which could serve as a signaling modality to induce hierarchical alignment and provide sufficient layers for cell infiltration and growth. These fibers were found to align circumferentially along the tubular scaffold where multiple layers are formed similar to that of the native tunica media layer. In addition the diameter of the fibrous mesh can be tune to suit various blood vessel dimension, *e.g.*, small caliber blood vessel with diameter <6 mm or large caliber blood vessel with diameter >6 mm. We have demonstrated in this study the flexibility of the auxiliary setup in tuning the dimension of the tubular scaffold. Fibres were collected in an optimized solvent bath *via* a conductive rotating mandrel. The dimension of the rotating mandrel would determine the diameter of the tubular scaffold. In addition, fibres collected in the solvent bath, placed directly underneath the spinneret were found to have higher porosity compared to the conventional electrospinning setup. The physical properties of the 3D aligned fibrous scaffold were characterized and the morphology, proliferation and maintenance of human aorta smooth muscle cells phenotype were investigated.

Materials and methods

Scaffold fabrication

All electrospun scaffold were prepared on Nanofiber Electrospinning System, Nanon-01A along with the newly designed auxiliary setup, as shown in Fig. 1. Briefly, polycaprolactone (PCL) pellets (Capa™ 6800 with average molecular weight of 80 000 amu) purchased from Perstorp was dissolved in 6.5 : 3.5 ratio of dichloromethane (DCM) and dimethylformamide (DMF) magnetic stirred for 24 hours to obtain a 13 wt% polymer solution. Polymer solution was fed at a rate of 0.5 to 1.0 ml h^{-1} to a flat tip stainless steel spinneret which is connected to a high-voltage power supply. Electrospinning was carried out at ambient temperature (20–24 °C) and at a range of accelerating voltage from 16 to 21 kV, while the collector remained earthed.

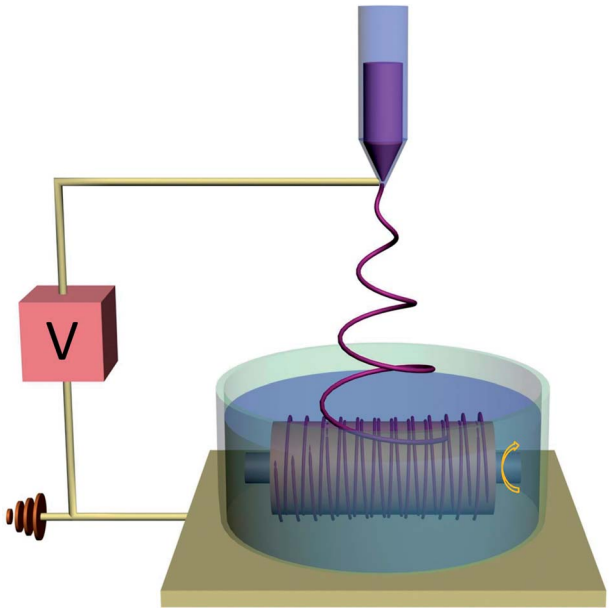

Fig. 1 Schematic illustration of the electrospinning auxiliary setup for the fabrication of 3D aligned fibrous scaffold with a tunable substrate collector.

The PCL polymer solution was pumped to a 21-gauge needle with a collector distance optimized between 4 to 20 mm. The rotation speed for collection of 3D aligned fibers was optimized between 500 to 800 rpm, while the collection of 3D random scaffold was performed without any form of rotation. The bath solution used in this study has been optimized based on an investigation of wettability between the polymer solution and the bath solution[32] (see ESI†). The concentration of 50 : 50 isopropyl alcohol (IPA) and deionized water was found to promote the infiltration of fibers into the collector bath making the scaffold more porous as compared to the conventional electrospinning process. All scaffolds were collected after 30 min of spinning with 5 min of cleaning frequency and placed in freezer for approximately 24 h prior to freeze drying.

Scaffold characterization

Scaffold morphology. Electrospun scaffolds were visualized with an Jeol 6360 thermionic scanning electron microscopy (SEM) or Jeol 6340F field emission scanning electron microscopy (FE-SEM) for close-up images. The samples were imaged at accelerating voltage of 5 kV and a working distance between 10-15 mm. All samples were coated with gold prior to imaging to increase the sample conductivity. Scaffolds were immersed in liquid nitrogen for 5 min, sectioned across the thickness prior to imaging the cross-sectional view.

2D fast Fourier transform (FFT) alignment. Fast Fourier transform (FFT) was performed to determine the fibre alignment in electrospun scaffold. The SEM image was uploaded to ImageJ® software where the image is processed by 2D FFT.[33] The resulting frequency plot would contain a cluster of white pixels depending on the nature of the image processed. Following which a rotation of 90° on the frequency plot was performed to correct for the inherent rotation of the data

induced by FFT analysis. The frequency plot is then analyzed by a supported oval profile plugin where the pixel intensities are summed along the radius for each angle of circular projection, *e.g.*, 0–360° and normalized to a baseline value of 0. Peaks of nearly uniform height is a characteristic of scaffold containing random features, while a highly aligned fibre scaffold would produce prominent peak in the 2D FFT alignment plot.

Scaffold porosity and pores. The scaffold porosity was measured by liquid intrusion method[15,34] where the weight of dry scaffold was first measured prior to immersion in 100% ethanol overnight. The scaffold was gently wiped to remove any excess ethanol on the surface and weighed again. Scaffold with ($n = 3$) was calculated with the following equations:

$$\text{Scaffold porosity} = \frac{V_{\text{eth}}}{\left(V_{\text{pcl}} + V_{\text{eth}}\right)} \times 100\%$$

where:

$$V_{\text{eth}} = \frac{\left(W_{\text{wet}} - W_{\text{dry}}\right)}{\rho_{\text{eth}}}$$

$$V_{\text{pcl}} = \frac{W_{\text{dry}}}{\rho_{\text{pcl}}}$$

V_{eth} denotes the volume of ethanol entrapped in the scaffold; W_{dry} and W_{wet} denote the dry and wet weight of the scaffold respectively; ρ_{eth} denotes the density of ethanol (0.789 mg mm^{-3}). ρ_{pcl} denotes the density of polycaprolactone (1.145 g cm^{-3}).

The average pore size of the scaffold was determined by measuring at least 50 pores per sample using the ImageJ® (NIH, Bethesda, Maryland, USA) software. The pore size is defined as the distance between fibres and expressed as mean ± standard deviation.

Contact angle measurement. The hydrophobicity of the 3D aligned and random scaffold was measured using the static water contact angle (WCA) technique on Dataphysics OCA system. Briefly, a G25 gauge needle was used to generate the sessile droplet at a volume of 6.0 μl and dosing rate of 1.0 μl s^{-1}. One droplet of distilled water was dropped on each sample ($n = 3$) where the projected images of droplet settled on the fibrous scaffold showing no noticeable changes was analyzed. The SCA 20 software was used to profile the droplet and the contact angle measurement was read off.

Mechanical properties. The aligned and random scaffolds were fabricated and cut according to ASTM D638 dimensions. Mechanical properties of aligned scaffolds were measured along the fibre direction (‖). The cross-sectional area of the samples ($n = 5$) were measured using micrometer and loaded onto an Instron 5567 testing machine, where testing were conducted using 10 N load and crosshead speed of 10 mm min^{-1}. The gauge length was determined as the distance between the grips. All testing were carried out at ambient temperature. Strain was determined as extension normalized to gauge length; stress was calculated as the load normalized to initial cross-sectional area. Modulus was computed as the slope of stress–strain curve.

Cell-scaffold interactions

Cell culture and seeding

Human aorta smooth muscle cells (hSMCs) used in this study was obtain from Lonza Clonetics® and expanded up to passage 7 to 9 on gelatin coated culture flasks. Cells were maintained in SmBM basal medium along with supplemented growth factors kit from Lonza and 1% antibiotic-antimycotic (AA) at 37 °C with 5% CO_2. For cell seeding, fibrous membrane upon freeze drying were cut to fit into 24 well plate, soaked in 70% ethanol for 1 hour, sterilized by UV irradiation for 1 hour on each side and rinsed in PBS three times. The membranes were incubated overnight with cell culture prior to cell seeding. The hSMCs were seeded onto the fibrous scaffolds at a density of 3×10^5 cells per well for cell morphology, proliferation and qualitative differentiation studies. The medium was refreshed every other day.

Cell proliferation

Cell proliferation was analyzed by WST-8 assay (Dojindo Molecular Laboratories Inc., Kumanoto, Japan). Briefly, on day 1, 4, 7 and 14 the medium was aspirated, and the cell culture medium in each well is replaced with 1 ml of medium with 10% of WST-8 reagent. The reaction was incubated at 37 °C and 5% CO_2 for 2 h. After which, 100 μl aliquots of each well were transferred to a fresh 96 well plate where absorbance readings were taken at 450 nm on a microplate reader. Each experiment were performed in triplicate.

Cell morphology analysis

The morphology of smooth muscle cells was studied after 1, 7 and 21 days of culture where the filamentous actin (F-actin) and cell nucleus were counter stained with rhodamine-phalloidin (1 : 200 dilution in 5% BSA, Life Technologies) and 4′-6-diamidino-2-phenylindole (DAPI) (1 : 1000 dilution in 5% BSA, Life Technologies) respectively. Briefly, hSMCs were fixed with 4% paraformaldehyde for 10 min at room temperature. The cells were permeabilized with 0.1% Triton X-100 in PBS for 10 min at room temperature and subsequently blocked with 5% bovine serum albumin (BSA) in PBS before the subcellular components were immune-labeled. The fluorescence images were visualized under a fluorescence microscope (CX 51; Olympus, Japan).

Immunocytochemistry analysis

The expression of early and late markers by the hSMCs, namely α-smooth muscle actin (α-SMA) and heavy myosin chain (MHC) respectively, were evaluated using immunocytochemistry analysis. Cells were fixed with 4% paraformaldehyde in PBS for 10 min at room temperature, washed 3 times in PBS and permeabilized with 0.1% Triton X-100 in PBS for 10 min at room temperature. After three washes with PBS, the cells were blocked with 10% goat serum (normal, Dako, Denmark) for 1 h. The samples were subsequently incubated with mouse monoclonal anti alpha smooth muscle actin (ab7817) (1 : 400, abcam)

and rabbit polyclonal anti smooth muscle myosin heavy chain 11 (ab53219) (1 : 200, abcam) overnight at 4 °C. Alexa Fluor secondary antibodies 488 goat anti-mouse IgG (1 : 200, Molecular probes, Invitrogen) and 568 goat anti-rabbit IgG (1 : 100, Molecular probes, Invitrogen) were used to counter stained its respective antibodies. Nuclei were stained with DAPI (1 : 1000 dilution in 5% BSA, Life Technologies). The fluorescence images were visualized under a fluorescence microscope (CX 51; Olympus, Japan).

Statistical analysis

Results are presented as mean ± standard deviation where statistical differences are determined by student's *t*-test and are considered statistically significant at $p \leq 0.01$.

Results and discussion

Design and collection of three-dimensional aligned fibrous scaffold

The electrospinning auxiliary setup designed in this study aims to collect tunable 3D aligned fibrous scaffold on a tubular format. The aligned fibres served as a signaling modality for the regulation and maintenance of SMCs contractile phenotype.[35,36] Well-aligned and porous scaffold were collected on the auxiliary electrospinning setup where fibres are aligned circumferentially on a tubular format and at the same time with sufficient substrate thickness. Fig. 2 presents the electrospinning setup and the macroscopic images of the tubular scaffold. The white Teflon bath was used to prevent fibers from attaching to the edges of the bath, while the stainless steel needle-like collector (Fig. 2a) was attached to a rotating mechanism for the collection of circumferentially aligned fibres. An additional advantage of the setup is the flexibility of tuning the diameter of the tubular construct. As a demonstration, tubular construct with diameter ~1 mm and 5 mm were made (Fig. 2c), these diameter was chosen to represent small and large caliber blood vessels respectively.

The bath solution has been optimized using the Wilhelmy plate method[32] described in ESI 1.† Briefly, in order to form 3D fibrous scaffold structure, fibres have to be deposited in a bath of solution that enhanced deposition and dispersion of fibres rather than a simple deposition on a conventional collector. The bath solution in this context would need to have surface tension value lower than the polymer solution. In this aspect, the electrospinning solution containing 13 w/v% of PCL in 6.5 : 3.5 ratio of dichloromethane (DCM) and dimethylformamide (DMF) was found to be 32.44 mN m^{-1}, any bath solution composition lower than this value is deem favorable for the process. It has been observed that bath solution containing 50% IPA in deionized water or higher is suitable for the wet electrospinning process. In addition, we have also observed that, bath solution has to be at least 6 mN m^{-1} lower than the electrospinning solution in order for fibres to be successfully deposited into the bath and get collected on the rotating mandrel. Bath solution having too low of surface tension would cause a deformed morphology of fibres, therefore we have optimized the bath solution to be in the regime of 6 to 9 mN m^{-1} lower than the electrospinning solution; more information is provided under the ESI 1.†

Morphology of 3D electrospun scaffold

To assess the morphology of electrospun fibres, SEM images were captured on 3D aligned and 3D random scaffolds. Fig. 3 presents the top, cross-sectional view as well as close-up FE-SEM images of the scaffolds. The SEM images revealed that scaffold fabricated on the auxiliary setup demonstrated higher porosity and thicknesses, the 3D aligned scaffold were found to be preferentially aligned along the rotating axis as shown in Fig. 3a. The fibre thickness and porosity of the aligned scaffold were comparable to the random scaffold, Fig. 3b. Cryo-sectioned images of the scaffold demonstrated that the 3D aligned scaffold present several layers of preferentially aligned fibres forming a tubular construct. This morphology is similar to the native tunica media layer found in blood vessel.[5,35] In addition, scaffolds made from the auxiliary setup could collect fibrous scaffolds with thickness in the range of 500–600 μm (Fig. 3c and d) as compared to only 100–200 μm when fabricated on conventional setup. Close-up images were taken on aligned scaffold where fibres were found to be smooth with no presence of pits and voids on the fibre, presenting a consistent substrate for future cell studies.

Physical properties of 3D electrospun scaffold

2D Fast Fourier transform alignment. The alignment of fibres were quantified with 2D fast Fourier transform (FFT) by

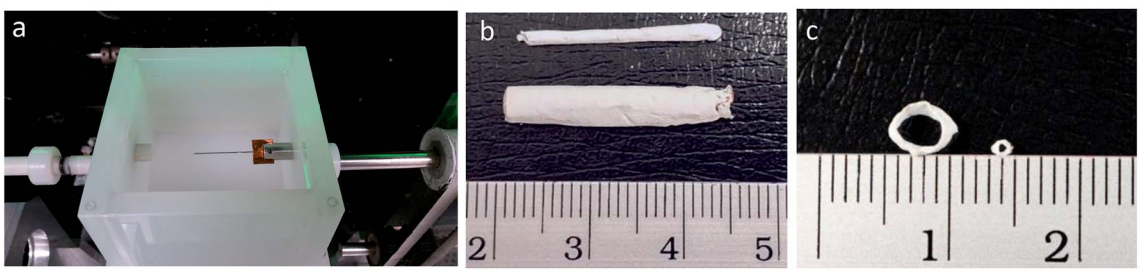

Fig. 2 Electrospinning auxiliary setup and macroscopic images of tubular scaffold. (a) Left, electrospinning auxiliary setup with tunable diameter stainless steel electrode. (b) Macroscopic images of tubular scaffold, showing typical length of scaffold. (c) Cross-sectional view of tubular scaffold, indicating the tunability of scaffold diameter.

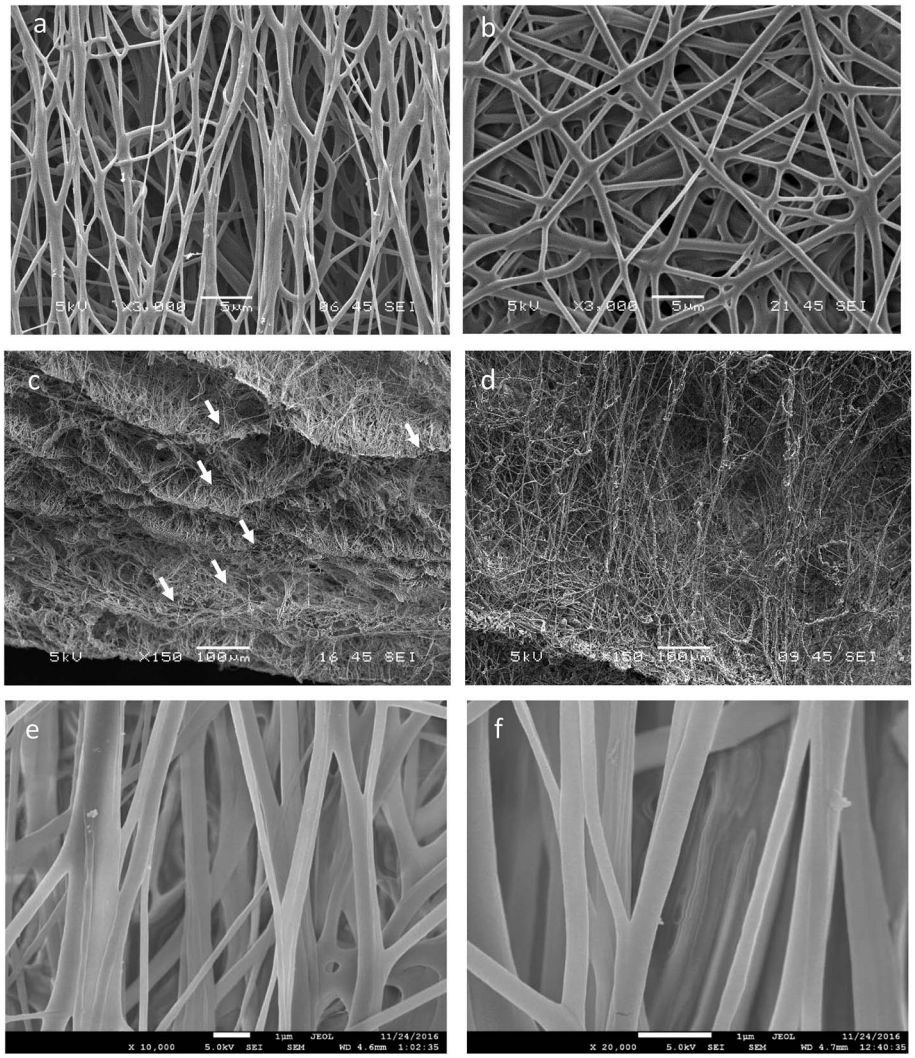

Fig. 3 SEM images of 3D aligned and random scaffolds. (a) Top view of 3D aligned fibrous scaffold exhibiting preferential alignment along rotation axis. (b) Top view of 3D random fibrous scaffold with no orientation preference. (c) Cross-sectional view of 3D aligned fibrous scaffold exhibiting multiple layers of aligned scaffold. (d) Cross-sectional view of 3D random fibrous scaffold. (e) FE-SEM images of 3D aligned fibrous scaffold at 10k× and (f) 20k× with smooth and homogenous fibre morphology.

converting the distribution of fiber orientation from image space to frequency space through an Image J® software. This plot consists of grayscale pixels distributed into a pattern that can be used to measure the degree of fibre alignment.[33,37] The frequency pixels were found to be predominately distributed along the vertical axis for 3D aligned scaffold, Fig. 4a, indicating a preferential alignment. However, the FFT frequency plot for 3D random scaffold, Fig. 4b, contain frequency pixels that are concentrated in the center with some high frequency pixels placed away from the origin. The peripheral frequency pixel correspond to edges, details and noise in the SEM image as a result of the high porosity nature found in 3D scaffolds.[33] The radial intensity summed using an oval-profile plugin was plotted against the angle of acquisition to obtain the FFT alignment plot, Fig. 4c. The peaks on the FFT alignment plot are narrow and sharply outlined, indicating a good degree of fibre alignment for the 3D aligned scaffold, while the nearly uniform peak height is a hallmark of scaffold consisting of random element as shown in 3D random scaffolds.[38]

Scaffold porosity and pore size. The porosity and pore size of a scaffold is essential to provide sufficient cellular infiltration and tissue ingrowth.[34,39] The liquid displacement method has been used to determine the porosity of the scaffold where the porosity of 3D aligned scaffold was found to be 94.09 ± 0.009% and 3D random scaffold to be 97.75 ± 0.006%. Both 3D aligned and random scaffolds were considerably porous, permitting cells infiltration and exchange of nutrients. The pore size of the two sets of scaffolds were measured on Image J® software where the average pore size for 3D aligned scaffold was determined to be approximately 11.63 ± 3.53 μm and 3D random scaffold with 10.623 ± 3.65 μm pore size. Fig. 4d and e presents the distribution curve of the measured pore size for 3D aligned and 3D random scaffold respectively.

Contact angle measurement. The static water contact angle (WCA) measurement has been performed on 3D aligned and

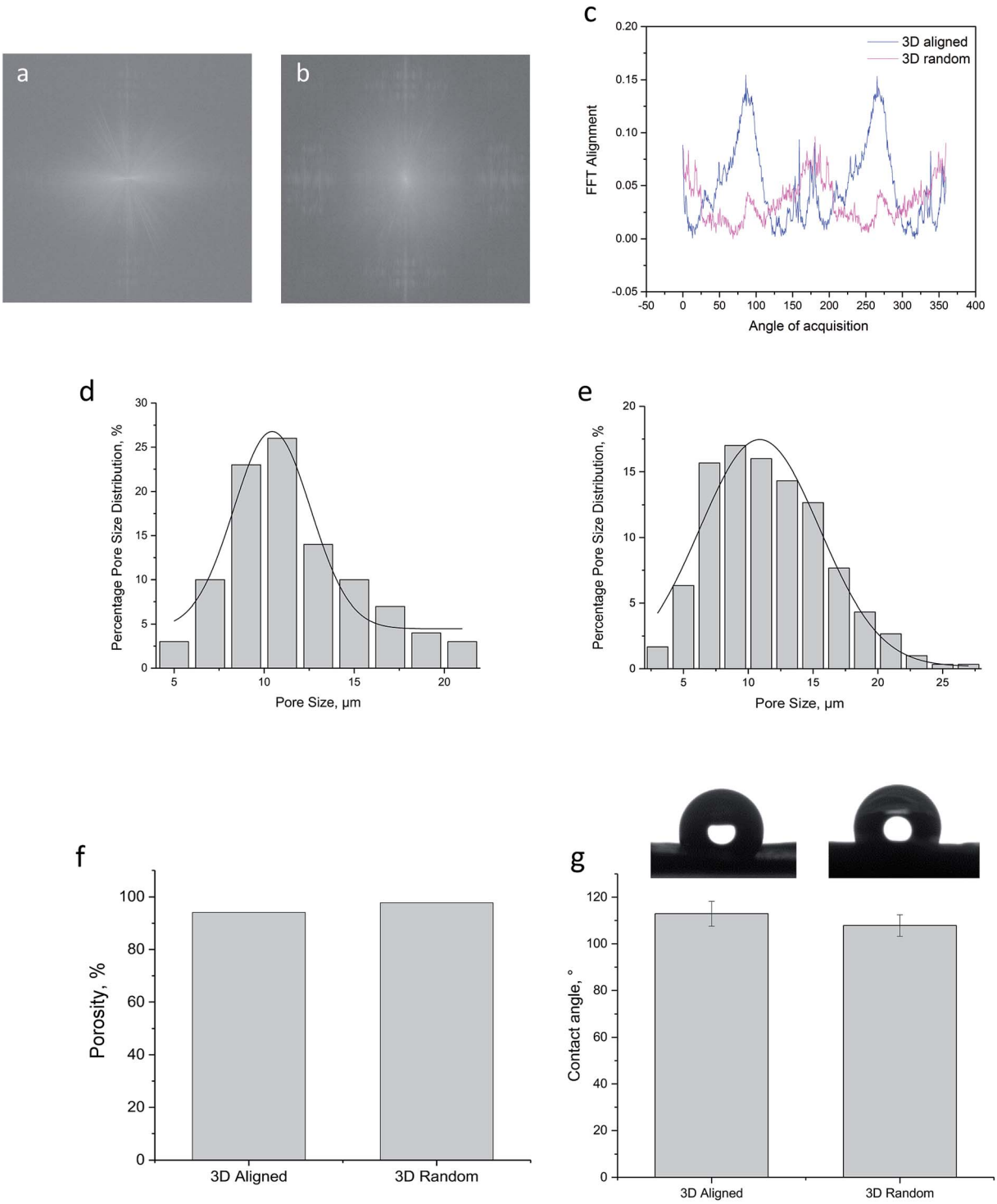

Fig. 4 Physical properties of 3D electrospun scaffold. (a) FFT frequency image of 3D aligned scaffold. (b) FFT frequency image of 3D random scaffold. (c) Combined FFT alignment plot. (d) Percentage pore size distribution plot for 3D aligned scaffold. (e) Percentage pore size distribution plot for 3D random scaffold. (f) Porosity bar chart for 3D aligned and 3D random scaffold. (g) Contact angle measurement chart for 3D aligned and 3D random scaffold.

random scaffold to determine the hydrophobicity of the uncoated porous scaffold. Polycaprolactone (PCL) used in this study is inherently hydrophobic where the static WCA of the film was reported to be 137 ± 2°.[40] In this study, the static WCA measured on 3D aligned scaffold was found to be 112.9 ± 5.3° and 107.83 ± 4.6° for 3D random scaffold. These values were significantly lower than the static WCA values reported for PCL film. The effect can be attributed to the excessive pores found in

Table 1 Mechanical properties of 3D aligned and 3D random scaffold

Scaffold properties	3D aligned	3D random
Tensile stress, kPa	1183.9 ± 144.48	86.08 ± 23.32
Young's modulus, kPa	16.99 ± 1.171	0.20 ± 0.078

3D scaffolds where larger pores and porosity formed on the 3D scaffolds promoted the infiltration of water hence reducing the hydrophobic effect of the scaffold.[41]

Mechanical properties. The mechanical properties of the scaffolds were evaluated to ensure sufficient substrate stiffness for further handling. The average tensile stress of 3D aligned scaffold conducted along the fibre direction was found to be 1183.9 ± 144.48 kPa and 86.08 ± 23.32 kPa for 3D random scaffold. Young's modulus of the aligned 3D scaffold (||) was found to be 16.99 ± 1.17 kPa while the 3D random scaffold was found to be 0.2 ± 0.08 kPa. It can be expected that the alignment of fibres in the 3D aligned scaffold contributed significantly to its mechanical properties. Although these mechanical values were much lower than many of the reported data[42,43] for 2D PCL scaffolds, it remained reasonable since the excessive pores formed during wet electrospinning could render a weaker scaffold structure as compared to the reported 2D scaffolds, see Table 1.

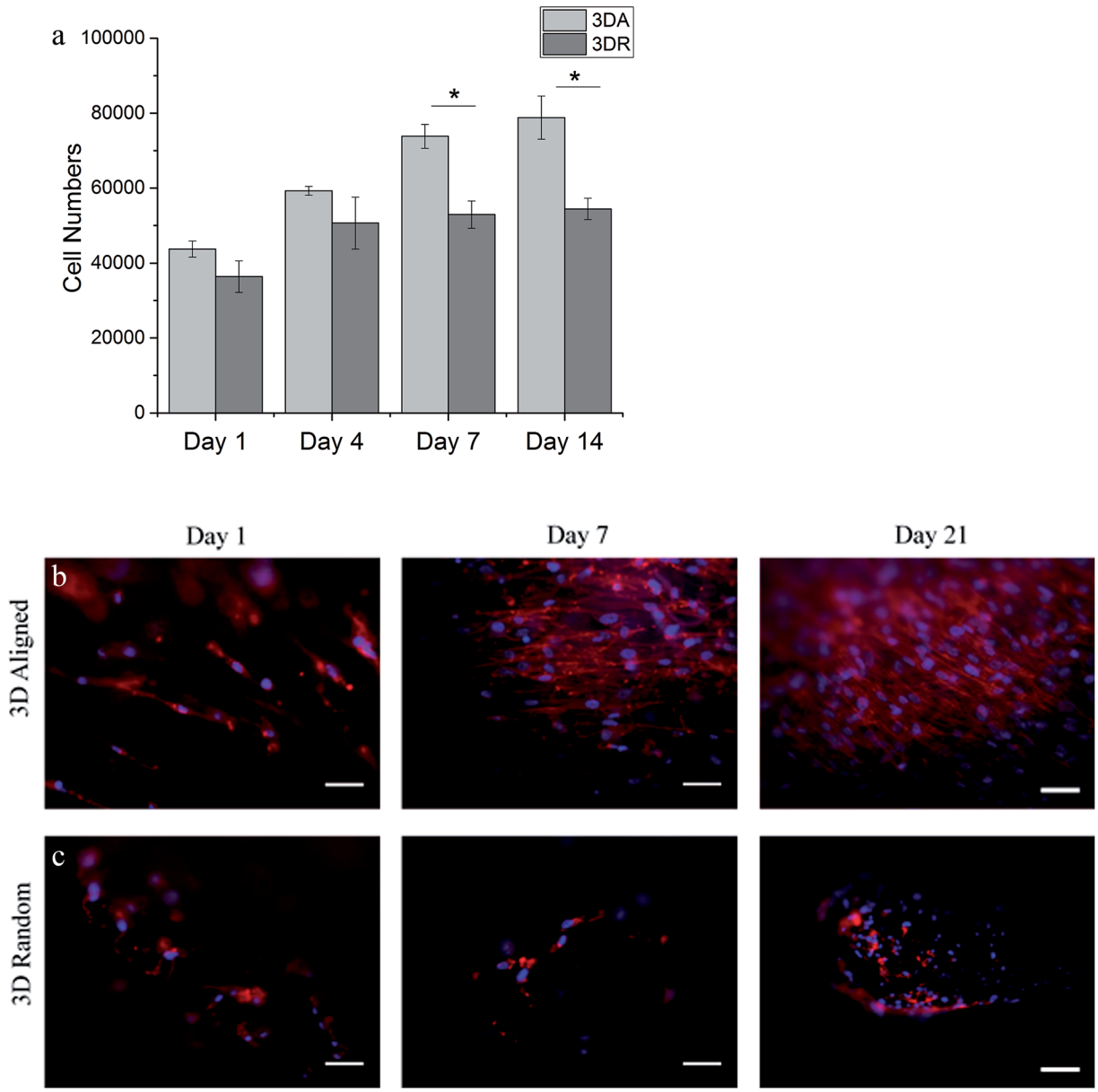

Fig. 5 Human SMCs proliferation and morphology studies on 3D aligned and 3D random scaffold (as denoted by 3DA and 3DR respectively). (a) Proliferation of hSMCs on 3D aligned and 3D random scaffold at 1, 4, 7 and 14 days of culture. *$p < 0.01$. (b) Fluorescence images of hSMCs on 3D aligned and (c) 3D random scaffold after 1, 7 and 21 days of culture. The actin filaments and nuclei of hSMCs were stained with rhodamine phalloidin (red) and DAPI (blue) respectively. (Scale bar = 50 μm).

Cell proliferation and morphology studies. Cell proliferation and morphology studies were assayed on the respective substrate to evaluate the effect of hSMCs on different substrate topography. The results showed that cell numbers increased significantly for 3D aligned scaffold after 7 days of culture ($p < 0.01$) indicating a higher proliferation ability, Fig. 5a. The cell number however remained relatively constant after 7 days of culture for both 3D aligned and 3D random scaffold. A further observation on cell morphology shown in Fig. 5b and c indicates that 3D aligned scaffold supported more elongated and spindle like shape morphology with preferential cell alignment along fibre axis. Such a cell-shape directionality is similar to the native SMCs found in vascular media layer,[2,35] it also indicates the contact guidance effect of the underlying substrate supporting cells alignment along fibre axis.[14] hSMCs grown on 3D random scaffold however remained round after 21 days of culture, the cells did not appear to be spreading or growing into the spindle cell shape indicating a lack in the ability of promoting a contractile phenotype.[13,14,44] Since promoting of well-differentiated contractile SMCs phenotype is one of the approach in minimizing the development of vascular pathologies,[6,35] cells grown on 3D aligned scaffold presents an alternative to maintain the contractile phenotype of hSMCs.

Phenotypic expression *in vitro*. Further cell studies were conducted to determine the phenotype of hSMCs in *in vitro* culture. The characteristic of contractile protein expression in hSMCs is the presence of alpha smooth muscle actin (α-SMA) and smooth muscle myosin heavy chain (MHC).[8,23,45] While α-SMA is the first known protein expressed during the early stages of SMCs differentiation, it is less definitive.[46] MHC on the other hand is a late protein marker during hSMC development and it served as an exclusive marker to identify SMC specificity.[35,45] Fig. 6 presents the immunofluorescent staining images of scaffold seeded with hSMCs after 21 days of culture. hSMCs cultured on 3D aligned fibrous substrate were found to exhibit definitive α-SMA and MHC markers that are orderly organized as microfilament bundles. The result suggest that 3D aligned fibrous scaffold could promote the maintenance of hSMCs contractile phenotype *in vitro*.[2,10,36] A relatively low degree of protein expression and irregularity has been observed on 3D random scaffold. The hSMCs did not appear to proliferate and immunostaining result suggest that cells were probably in their synthetic phenotype since there were limited expression of MHC. This observation is consistent with the cell morphology findings since hSMCs cultured on 3D random scaffold failed to exhibit the typical spindle elongated contractile morphology. Therefore, the positive expression of α-SMA and MHC on 3D aligned fibrous scaffold suggest that hSMCs were able to retain its functionality on such *in vitro* culture.

Discussion

One of the limitations in achieving a successful engineered vascular grafts lies in the regulation of hyperplastic vascular smooth muscle cells (vSMCs) into a contractile phenotype.[10,47] It has been reported that occlusion (thrombus formation) during the early stages of implantation followed by excessive tissue ingrowth (intimal hyperplasia) is the main cause of graft failure especially in small diameter vascular grafts.[35,36,48] The regulation of vSMCs into its contractile phenotype is one of the strategy to minimize vascular pathologies since the regeneration of healthy native-like tunica media layer could potentially protect and support the growth of endothelial cells and improve overall graft patency.[17,49] The regulation of vSMCs has been attempted by various groups broadly by means of adopting the use of

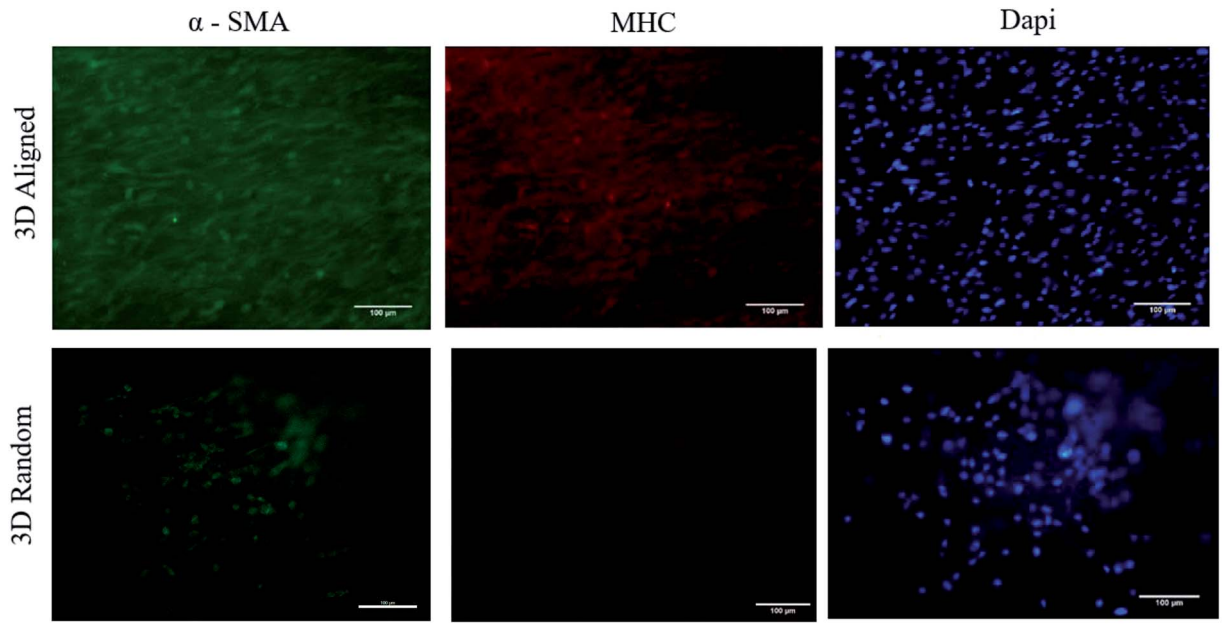

Fig. 6 Immunofluorescent staining images of α-SMA and MHC expressions of human SMCs after 21 days of culture. Cells were stained using mouse monoclonal anti alpha smooth muscle actin (α-SMA) (green), rabbit polyclonal anti smooth muscle myosin heavy chain (MHC) 11 (red), and DAPI (blue). (Scale bar = 100 μm).

soluble signaling factors,[50,51] mechanical stimulation[9,45] or co-culturing of cells (*e.g.* endothelial cells).[21,49] While each of these methods exhibits its pros and cons we are particularly interested in regenerating vascular tissue by engineering the tunica media layer where fibres were found to align circumferentially.[2,35] This native-like architecture presents the vSMCs a favorable site for repair and regeneration where the cell-free graft could take advantage of its host self-remodeling ability and prevent potential host rejections. Although there were many reports on the fabrication of fibrous scaffold for vascular tissue regeneration, there were limited report on the fabrication of 3D aligned fibrous scaffold on a tubular format.[4,15,23,52] Considering the requirement of fiber alignment on smooth muscle cell function along with providing sufficient 3 dimensionality for tissue remodeling, an innovative setup has been designed in this study to address the current limitation. The electrospinning setup designed in this study has enabled the collection of circumferentially aligned scaffold on a tubular format, Fig. 1. The aligned fibrous scaffold that has been collected in a bath of solvent solution has been optimized by the Wilhelmy plate method[32] as described in the ESI.† Fibres that entered the bath solution were aligned circumferentially along the collector pin and due to the presence of bath solution, fibres collected were found to be much porous as compared to the conventional 2D electrospinning. Additional advantage of the auxiliary setup lies in the flexibility of tuning the dimension of the tubular construct. The collector pin used in this study would determine the final diameter of the construct, and we have demonstrated the flexibility of fabricating tubular construct for both small and large caliber blood vessels with diameter of approximately 1 mm and 6 mm respectively, Fig. 2b and c. To the best of our current knowledge, no report has demonstrated the fabrication of 3D aligned, porous and fibrous scaffold formed on a tubular format with additional tunability of its construct diameter. The added scaffold diameter and thickness tunability is deemed as an attractive advantage since the grafts can be tailored to the needs of individual patients.[5,35]

Prior to cell studies, physical characterization of the scaffold has been performed on both 3D aligned and 3D random scaffolds made from the electrospinning auxiliary setup. From the SEM micrographs, 3D aligned scaffold demonstrated satisfactory alignment along the collector pin rotation axis, while 3D random scaffold retained its random nature. The alignment of fibres formed on 3D scaffold was considered an important feature to induce hierarchical alignment for smooth muscle cells. Although both 3D aligned and 3D random scaffold exhibited sufficient substrate thickness, the 3D aligned scaffold demonstrated an additional advantage with its multiple layer of fibres wrapping along the collector pin; this micro-architecture was found to be similar to the native media layer.[4,45] Further fibre alignment quantification confirmed a good degree of fibre alignment for 3D aligned scaffold with presence of prominent peaks seen on the FFT alignment plot. The porosity measurement of both scaffold *via* the liquid displacement method indicated relatively similar and high porosity value. Similar trend was observed for the average pore size distribution and static water contact angle measurement. Collectively from the physical characterization data, both 3D aligned and 3D random scaffold exhibited relatively similar properties, leaving the effect of fibre alignment on hSMCs function to be the main differentiating factor.

From the *in vitro* cell studies, hSMCs appeared to be well supported by 3D aligned scaffold with increased in cell proliferation ability and enhanced cell-shape directionality.[8,13,14,25] hSMCs cultured on 3D aligned scaffold exhibited an elongated and spindle-type cell shape with preferential cell alignment along the fibre axis, Fig. 5. The cell-shape directionality was found to be similar to the native SMCs residing in the vascular media layer, indicating a conducive cell-scaffold interaction for the maintenance of contractile phenotype.[14,35] On the other hand, hSMCs grown on 3D random scaffold remained round and exhibited a synthetic-like morphology even up to 21 days of culture; the cells did not appear to be spreading or growing into the spindle cell shape indicating a lack in the ability of promoting a contractile phenotype.[13,23] Since promotion of well-differentiated contractile SMCs phenotype is one of the approaches in minimizing the development of vascular pathologies, cells grown on 3D aligned scaffold presents a better alternative to maintain the contractile phenotype of hSMCs. Further investigation were performed to determine the functional expression of two representative intracellular contractile proteins of hSMCs (*i.e.* α-SMA and MHC). hSMCs cultured on 3D aligned fibrous scaffold were found to exhibit definitive α-SMA and MHC markers that are orderly organized as microfilament bundles, Fig. 6. This result is consistent since an elongated spindle-like cell shape is an indication of cell contractile nature,[8,45] hence an increased expression and organization of the contractile protein marker would be expected on 3D aligned scaffold. A relatively low degree of protein expression and irregularity has been observed on 3D random scaffold. The hSMCs did not appear to proliferate and immunostaining result suggest that cells were probably in their synthetic phenotype since there were limited expression of MHC, a late marker of vSMCs.

Knowing that the regulation of vSMCs differentiation is integral to minimize vascular pathologies such as intimal hyperplasia, the results presented henceforth is exciting since the topographical cues presented by 3D aligned scaffold were capable of inducing hierarchical alignment and definitive α-SMA and MHC markers. The result suggest a substantial possibility of adapting the 3D aligned tubular scaffold to enhance and regulate cell function. In addition, the tunability of scaffold diameter and thickness present an additional advantage for tailoring to the needs of individual patients or future *ex vivo* studies.[5,35]

Conclusion

In this study, we presented the design of an electrospinning auxiliary jig that enabled the collection of circumferentially aligned scaffold on a 3D tubular format. The 3D aligned fibrous scaffold formed on the electrospinning auxiliary jig were found to be porous with preferential alignment confirmed by 2D FFT approach. The construct which comprise of several layers of aligned fibres mimics the native tunica media layer of blood

vessel. The maintenance of vascular smooth muscle cells (vSMCs) on such micro-architecture substrate is vital for successful graft replacement. Herein the fabricated 3D aligned fibrous scaffold seeded with hSMCs exhibited enhanced cell proliferation ability, cell-shape directionality and definitive contractile protein expression of α-SMA and MHC. The additional flexibility of tuning the dimension of construct makes it a promising approach as a personalized treatment for individual patients or future *ex vivo* studies.

Conflicts of interest

There are no conflicts to declare.

Acknowledgements

This work is supported in part by the Singapore Institute of Manufacturing Technology, Science and Engineering Research Council, Agency for Science, Technology and Research (A*STAR) Singapore; MOE Tier 1 RG46/18 funding; FL NG is an A*STAR Graduate Research Scholar. HZ CHEN is a NTU Interdisciplinary Graduate Research Scholar.

References

1 P. L. Schnall, M. Dobson and P. Landsbergis, *Int. J. Health Serv.*, 2016, **46**, 656–692.
2 W. G. Chang and L. E. Niklason, *NPJ Regen. Med.*, 2017, **2**, 7.
3 A. A. M. Ali, P. Sharma, R. N. Rege, S. Rajesh and K. Nadhamuni, *Indian J. Radiol. Imaging*, 2016, **26**, 472–474.
4 Y. Zhang, X. S. Li, A. G. Guex, S. S. Liu, E. Müller, R. I. Malini, H. J. Zhao, M. Rottmar, K. Maniura-Weber, R. M. Rossi and F. Spano, *Biofabrication*, 2017, **9**, 025010.
5 G. H. Borschel, Y. C. Huang, S. Calve, E. M. Arruda, J. B. Lynch, D. E. Dow, W. M. Kuzon, R. G. Dennis and D. L. Brown, *Tissue Eng.*, 2005, **11**, 778–786.
6 W. E. Burkel, *Med. Prog. Technol.*, 1988, **14**, 165–175.
7 R. H. Schmedlen, W. M. Elbjeirami, A. S. Gobin and J. L. West, *Clin. Plast. Surg.*, 2003, **30**, 507–517.
8 J. A. Beamish, P. He, K. Kottke-Marchant and R. E. Marchant, *Tissue Eng., Part B*, 2010, **16**, 467–491.
9 S. Chang, S. Song, J. Lee, J. Yoon, J. Park, S. Choi, J. K. Park, K. Choi and C. Choi, *PLoS One*, 2014, **9**, e88089.
10 E. M. Rzucidlo, K. A. Martin and R. J. Powell, *J. Vasc. Surg.*, 2007, **45**(suppl A), A25–A32.
11 X. Zhao, S. A. Irvine, A. Agrawal, Y. Cao, P. Q. Lim, S. Y. Tan and S. S. Venkatraman, *Acta Biomater.*, 2015, **26**, 159–168.
12 R. G. Thakar, F. Ho, N. F. Huang, D. Liepmann and S. Li, *Biochem. Biophys. Res. Commun.*, 2003, **307**, 883–890.
13 Q. Zhou, J. Xie, M. Bao, H. Yuan, Z. Ye, X. Lou and Y. Zhang, *J. Mater. Chem. B*, 2015, **3**, 4439–4450.
14 H. Yuan, J. Qin, J. Xie, B. Li, Z. Yu, Z. Peng, B. Yi, X. Lou, X. Lu and Y. Zhang, *Nanoscale*, 2016, **8**, 16307–16322.
15 M. Zhu, Z. Wang, J. Zhang, L. Wang, X. Yang, J. Chen, G. Fan, S. Ji, C. Xing, K. Wang, Q. Zhao, Y. Zhu, D. Kong and L. Wang, *Biomaterials*, 2015, **61**, 85–94.
16 D. I. Braghirolli, V. E. Helfer, P. C. Chagastelles, T. P. Dalberto, D. Gamba and P. Pranke, *Biomed. Mater.*, 2017, **12**, 025003.
17 B. E. Sumpio, J. T. Riley and A. Dardik, *Int. J. Biochem. Cell Biol.*, 2002, **34**, 1508–1512.
18 E. D'Arcangelo and A. P. McGuigan, *BioTechniques*, 2015, **58**, 13–23.
19 P. Davoudi, S. Assadpour, M. A. Derakhshan, J. Ai, A. Solouk and H. Ghanbari, *Mater. Sci. Eng., C*, 2017, **80**, 213–221.
20 Y. Yao, J. Wang, Y. Cui, R. Xu, Z. Wang, J. Zhang, K. Wang, Y. Li, Q. Zhao and D. Kong, *Acta Biomater.*, 2014, **10**, 2739–2749.
21 D. J. Brown, E. M. Rzucidlo, B. L. Merenick, R. J. Wagner, K. A. Martin and R. J. Powell, *J. Vasc. Surg.*, 2005, **41**, 509–516.
22 X. Lin, Y. He, X. Hou, Z. Zhang, R. Wang and Q. Wu, *PLoS One*, 2016, 11.
23 N. Masoumi, B. L. Larson, N. Annabi, M. Kharaziha, B. Zamanian, K. S. Shapero, A. T. Cubberley, G. Camci-Unal, K. B. Manning, J. E. Mayer and A. Khademhosseini, *Adv. Healthcare Mater.*, 2014, **3**, 929–939.
24 A. Agrawal, B. H. Lee, S. Irvine, J. An, R. Bhuthalingam, V. Singh, K. Y. Low, C. Kai Chua and S. Venkatraman, *Smooth Muscle Cell Alignment and Phenotype Control by Melt Spun Polycaprolactone Fibers for Seeding of Tissue Engineered Blood Vessels*, 2015.
25 H. Ahn, Y. M. Ju, H. Takahashi, D. F. Williams, J. J. Yoo, S. J. Lee, T. Okano and A. Atala, *Acta Biomater.*, 2015, **16**, 14–22.
26 M. Centola, A. Rainer, C. Spadaccio, S. D. Porcellinis, J. A. Genovese and M. Trombetta, *Biofabrication*, 2010, **2**, 014102.
27 H. K. Wong, C. R. Ivan Lam, F. Wen, S. K. Mark Chong, N. S. Tan, C. Jerry, M. Pal and L. P. Tan, *Biofabrication*, 2016, **8**, 015004.
28 C. Y. Tay, S. A. Irvine, F. Y. Boey, L. P. Tan and S. Venkatraman, *Small*, 2011, **7**, 1361–1378.
29 A. Tamayol, M. Akbari, N. Annabi, A. Paul, A. Khademhosseini and D. Juncker, *Biotechnol. Adv.*, 2013, **31**, 669–687.
30 T. Dvir, B. P. Timko, D. S. Kohane and R. Langer, *Nat. Nanotechnol.*, 2011, **6**, 13–22.
31 H. Chen, Y. Peng, S. Wu and L. P. Tan, *Materials*, 2016, **9**(4), 272.
32 L. Q. N. Tran, C. Fuentes, I. Verpoest and A. W. Vuure, *Interfacial Compatibility and Adhesion in Natural Fiber Composites*, 2015.
33 C. E. Ayres, B. S. Jha, H. Meredith, J. R. Bowman, G. L. Bowlin, S. C. Henderson and D. G. Simpson, *J. Biomater. Sci., Polym. Ed.*, 2008, **19**, 603–621.
34 Q. L. Loh and C. Choong, *Tissue Eng., Part B*, 2013, **19**, 485–502.
35 M. B. Chan-Park, J. Y. Shen, Y. Cao, Y. Xiong, Y. Liu, S. Rayatpisheh, G. C. Kang and H. P. Greisler, *J. Biomed. Mater. Res., Part A*, 2009, **88**, 1104–1121.
36 B. C. Isenberg, C. Williams and R. T. Tranquillo, *Circ. Res.*, 2006, **98**, 25–35.

37 C. Ayres, G. L. Bowlin, S. C. Henderson, L. Taylor, J. Shultz, J. Alexander, T. A. Telemeco and D. G. Simpson, *Biomaterials*, 2006, **27**(32), 5524–5534.
38 J. I. Kim, T. I. Hwang, L. E. Aguilar, C. H. Park and C. S. Kim, *Sci. Rep.*, 2016, **6**, 23761.
39 J. Rnjak-Kovacina and A. S. Weiss, *Tissue Eng., Part B*, 2011, **17**, 365–372.
40 C. R. Reshmi, S. P. Sundaran, A. Juraij and S. Athiyanathil, *RSC Adv.*, 2017, **7**, 2092–2102.
41 W. J. Lau, O. Chi Siang, P. Goh, B. C. Ng and A. Ismail, *Preparation and characterization of PVDF–PVP–TiO_2 composite hollow fiber membranes for oily wastewater treatment using submerged membrane system*, 2015.
42 H. Xu and Y. Yang, in *Lightweight Materials from Biopolymers and Biofibers*, American Chemical Society, 2014, ch. 7, vol. 1175, pp. 103–126.
43 A. Elamparithi, A. M. Punnoose, S. Kuruvilla, M. Ravi, S. Rao and S. F. D. Paul, *Artif. Cells, Nanomed., Biotechnol.*, 2016, **44**, 878–884.
44 A. H. Chan, R. P. Tan, P. L. Michael, B. S. Lee, L. Z. Vanags, M. K. Ng, C. A. Bursill and S. G. Wise, *PLoS One*, 2017, **12**, e0174773.
45 S. S. Rensen, P. A. Doevendans and G. J. van Eys, *Neth. Heart J.*, 2007, **15**, 100–108.
46 G. K. Owens, M. S. Kumar and B. R. Wamhoff, *Physiol. Rev.*, 2004, **84**, 767–801.
47 A. C. Doran, N. Meller and C. A. McNamara, *Arterioscler., Thromb., Vasc. Biol.*, 2008, **28**, 812–819.
48 A. C. Thomas, G. R. Campbell and J. H. Campbell, *Cardiovasc. Pathol.*, 2003, **12**, 271–276.
49 M. Pasic, W. Muller-Glauser, L. von Segesser, B. Odermatt, M. Lachat and M. Turina, *Eur. J. Cardio-Thorac. Surg.*, 1996, **10**, 372–379.
50 P. Zhou, F. Zhou, B. Liu, Y. Zhao and X. Yuan, *J. Mater. Chem. B*, 2017, **5**, 9312–9325.
51 B. H. Rauch, E. Millette, R. D. Kenagy, G. Daum and A. W. Clowes, *Circ. Res.*, 2004, **94**, 340–345.
52 T. Fukunishi, C. A. Best, T. Sugiura, T. Shoji, T. Yi, B. Udelsman, D. Ohst, C. S. Ong, H. Zhang, T. Shinoka, C. K. Breuer, J. Johnson and N. Hibino, *PLoS One*, 2016, **11**, e0158555.
53 C. A. F. Le Quan Ngoc Tran, Ignace Verpoest, Aart Willem Van Vuure, in *Natural Fiber Composites*, ed. R. D. S. G.Campilho, Taylor & Francis Group, 2016, ch. 5, pp. 127–155.